Relativistic many-body perturbation calculations on extreme ultraviolet and soft-x-ray transition energies in siliconlike iron

Marius J. Vilkas and Yasuyuki Ishikawa
Department of Chemistry, University of Puerto Rico, P.O. Box 23346, San Juan, Puerto Rico 00931-3346, USA
(Received 9 January 2004; published 4 June 2004)

Relativistic multireference many-body perturbation theory is generalized to calculate the energies of highly excited levels in multivalence-electron ions of iron group elements responsible for soft-x-ray emission lines. Term energies of the highly excited $n=4$ states arising from the $3s^23p4l$ ($l=0-3$) and $3s3p^24l$ ($l=0-3$) configurations in Fe XIII are computed to high accuracy. Theoretical electric dipole transition probabilities and wavelengths of the transitions to low-lying $n=3$ levels are compared with solar and laboratory lines to identify hitherto unidentified and/or poorly characterized extreme ultraviolet and soft-x-ray spectral lines. $E1$, $E2$, and $M1$ decay rates and lifetimes of lower excited levels of the $n=3$ manifold are evaluated as a benchmark for future experiments.

DOI: 10.1103/PhysRevA.69.062503 PACS number(s): 31.15.Ar, 31.15.Md, 31.15.Ne, 31.25.Jf

I. INTRODUCTION

Astrophysical interest in the spectra of multiply charged ions has increased in recent years as satellite-borne telescopes and instruments expand the range of detectable radiation into the x-ray region. In particular, the studies of stellar and solar coronae have intensified as a result of quality data acquisitions by the Extreme-Ultraviolet (EUV) Explorer satellite, Chandra x-ray observatory, and the Solar Heliospheric Observatory (SOHO) that recorded superb coronal spectra [1,2]. The ultraviolet (UV) through EUV and soft-x-ray emission lines from multiply charged ions are particularly useful as they provide detailed knowledge of the coronal atmosphere. Whereas a wealth of spectra from solar corona has been recorded, about half of the UV-EUV lines remain unidentified [3–5].

Siliconlike ions of iron group elements have numerous prominent lines in the solar coronal and flare spectra. While the energy levels arising from the ground $3s^23p^2$ and excited $3s3p^3$ and $3s^23p3d$ configurations have been fairly well established in ions of the silicon isoelectronic sequence, a recent fast-beam spectroscopy experiment [6] and high-accuracy calculations [7,8] revealed a number of inconsistencies in earlier UV line identifications. In a recent study on the $3s^23p3d\ ^3F^o_{2,3,4}$ levels [7,8], we have shown that due to incorrect spectroscopic assignment of the observed UV lines, the deduced term energies of the Fe XIII $3s^23p3d\ ^3F^o_2$ and $^3F^o_3$ levels were incorrect. The term energies of the poorly characterized $3s^23p3d\ ^3F^o_{2,3,4}$ levels were theoretically determined to 0.01% accuracy. Critical evaluation of these levels is very important because a large number of the electric-dipole ($E1$) transitions originating from $n=4$ even-parity levels decay to the $3s^23p3d\ ^3F^o_{2,3,4}$ states.

EUV and soft-x-ray regions of the solar and laboratory spectra of multiply charged ions of iron group elements have been very poorly characterized. The paucity of well-characterized lines arises partly because extant theories have limited predictive power and accuracy for spectroscopic identification even on low-lying $n=3$ states, much less highly excited $n=4$ levels given the wealth of possible transitions. For the Fe XIII EUV and soft-x-ray emissions from the $3s^23p4l$ ($l=0-2$) states, spectroscopic assignments based on semiempiral calculations have been made on a limited number of lines in the earlier studies of Fawcett *et al.* [9] and Kastner *et al.* [10]. In fact, the term energies have been deduced from only a few observed lines, rendering the assignment tentative. A higher level of theory capable of providing accurate term energies must be brought to bear on the EUV and soft-x-ray spectra to identify hitherto unidentified laboratory and coronal lines or to critically evaluate experimentally identified lines.

In this study, we generalize the previous study [11] and develop a relativistic multi-reference Møller-Plesset perturbation theory (MR-MP) for accurate predictions of term energies of a large number of excited levels of $n=3$ and 4 manifolds in multivalence-electron ions of iron group elements responsible for the hitherto unidentified EUV and x-ray emissions. Theoretical transition energies and decay rates of over 4000 excited $n=3$ and $n=4$ levels in Fe XIII are evaluated to high accuracy and compared with solar and laboratory lines. Theoretical transition rates and lifetimes of low-lying $n=3$ excited states are reported as a benchmark for future lifetime measurements. A synthetic soft-x-ray spectrum of Fe XIII is generated based on theoretical energy levels and transition rates to explicate the wealth of soft-x-ray emission lines in a recently recorded spectrum [12] that extant spectral models fail to reproduce. The purpose of the present study is to develop a relativistic many-body perturbation theory (MBPT) for the theoretical EUV and x-ray spectroscopy of astronomically relevant ions.

II. METHOD

The major difficulty in developing a high-accuracy many-body algorithm for multivalence-electron systems lies in the near degeneracy of the valence shells and an accurate description of valence-core dynamic correlation. Multiconfiguration Dirac-Fock-Breit (MCDFB) self-consistent field (SCF) and configuration interaction (CI) methods are most effective in treating nondynamic correlation (i.e., near degen-

eracy in the valence shells) but fail to accurately account for the bulk of dynamic correlations in systems with a large number of electrons. Single-reference many-body perturbation theory has exactly the opposite characteristic; it is effective in accurately describing dynamic correlation but fails to account for nondynamic correlation. Dynamic correlation is a short-range effect that arises from electron-electron interactions and is the major correction to the Dirac-Fock (DF) independent particle model, while nondynamic correlation is a consequence of the existence of nearly degenerate excited states that interact strongly with the reference state [13].

Systems in which only the dynamic correlation is important may be described by a single-configuration DF wave function, whereas systems with significant nondynamic correlation cannot be correctly described within single-configuration DF wave functions. Near degeneracy in the valence shells gives rise to a manifold of strongly interacting configurations — i.e., strong configuration mixing within a relativistic complex [13]—and makes a MC treatment mandatory [14–16]. In an earlier study, we developed a combined state-averaged MCDFB SCF+state-specific MR-MP that accurately accounts for both nondynamic and dynamic correlation corrections. The combined method provides accurate term energies and lifetimes of over 80 excited levels of $n=3$ manifolds in ions of the iron group elements [7,8,11]. For highly excited levels of the $n=4$ manifold, however, the MCDFB SCF becomes quickly unwieldy, and the CI method is more straightforward [17–20] to account for the strong configuration mixing and to ensure an energy upperbound for the $n=4$ excited levels. With this in mind, we generalize the previous study and develop a combined many-body algorithm for high-accuracy calculations of highly excited states in multivalence-electron systems.

The method begins with a state-averaged MCDFB SCF for the ground and low-lying excited states in Fe XIII, to obtain a common set of core and valence spinors in the V^N potential. This is followed by a relativistic multireference CI method [21], including the highly excited states of the $n=4$ manifold, to account for a near-degeneracy effect or strong configuration mixing, among the excited levels in the spirit of Dzuba, Flambaum, and Kozlov [18] and Savukov and Johnson [19]. The relativistic CI, however, fails to account for the bulk of dynamic correlation among highly excited levels unless a very large number of configurations, on the order of 1×10^6, are included in the CI calculations. The residual dynamic correlation corrections, however, can easily be accounted for by state-specific MR-MP based on the CI wave functions. In the following subsections, the combined MCDFB/CI+MR-MP theory is briefly outlined.

A. MCDFB SCF calculations of core and valence spinors

The effective N-electron Hamiltonian (in atomic units) for the development of our relativistic MR-MBPT algorithm is taken to be the relativistic "no-pair" Dirac-Coulomb-Breit (DCB) Hamiltonian [22,23]

$$H^+_{DCB}=\sum_i h_D(i)+\mathcal{L}_+\left(\sum_{i>j}\frac{1}{r_{ij}}+B_{ij}\right)\mathcal{L}_+, \tag{1}$$

with

$$B_{ij}=-\frac{1}{2}[\boldsymbol{\alpha}_i\cdot\boldsymbol{\alpha}_j+(\boldsymbol{\alpha}_i\cdot\mathbf{r}_{ij})(\boldsymbol{\alpha}_j\cdot\mathbf{r}_{ij})/r_{ij}^2]/r_{ij}. \tag{2}$$

Here $h_D(i)$ is the Dirac one-electron Hamiltonian. The DCB Hamiltonian is covariant to first order and increases the accuracy of calculated fine-structure splittings and inner-shell binding energies. Higher-order QED effects appear first in order α^3. The nucleus is modeled as a sphere of uniform proton charge distribution: $\mathcal{L}_+=L_+(1)L_+(2)\cdots L_+(N)$, where $L_+(i)$ is the projection operator onto the space $D^{(+)}$ spanned by the positive-energy eigenfunctions of the matrix DFB SCF equation [23]. $\mathcal{L}_+$ is the projection operator onto the positive-energy space $\mathfrak{D}^{(+)}$ spanned by the N-electron configuration-state functions (CFS's) constructed from the positive-energy eigenfunctions of the matrix DFB SCF. It takes into account the field-theoretic condition that the negative-energy states are filled. The eigenfunctions $\{\phi^{(\pm)}_{n_q\kappa_q}(r)\}(\in D^{(+)}\cup D^{(-)})$ of the matrix DFB SCF equation clearly separate into two discrete manifolds $D^{(+)}$ and $D^{(-)}$, respectively, of positive- and negative-energy one-particle states. As a result, the positive-energy projection operators can be accomodated easily in many-body calculations. The formal conditions on the projection are automatically satisfied when only the positive-energy spinors are employed.

N-electron eigenfunctions of the no-pair DCB Hamiltonian are approximated by a linear combination of M_{MC} configuration-state functions $\{\Phi^{(+)}_I(\gamma_I\mathcal{J}\pi);I=1,2,\ldots,M_{MC}\}\in\mathfrak{P}^{(+)}$, constructed from positive-energy eigenfunctions of the matrix MCDFB SCF equation:

$$\psi^{MC}_K(\gamma_K\mathcal{J}\pi)=\sum_I^{M_{MC}} C_{IK}\Phi^{(+)}_I(\gamma_I\mathcal{J}\pi). \tag{3}$$

The MCDFB SCF wave function $\psi^{MC}_K(\gamma_K\mathcal{J}\pi)$ is an eigenfunction of the angular momentum and parity operators with total angular momentum $\mathcal{J}$ and parity π. Here γ denotes a set of quantum numbers other than $\mathcal{J}$ and π necessary to specify the state uniquely. The total DCB energy of the general state represented by the MC wave function $\psi^{MC}_K(\gamma_K\mathcal{J}\pi)$ can be expressed as

$$E^{MC}_{DCB}(\gamma_K\mathcal{J}\pi)=\sum_{IJ}^{\mathfrak{P}(+)} C_{IK}C_{JK}\langle\Phi^{(+)}_I(\gamma_I\mathcal{J}\pi)|H^+_{DCB}|\Phi^{(+)}_J(\gamma_J\mathcal{J}\pi)\rangle. \tag{4}$$

Here, it is assumed that $\psi_K(\gamma_K\mathcal{J}\pi)$ and $\Phi^{(+)}_J(\gamma_J\mathcal{J}\pi)$ are normalized.

The second-order variation of the state-averaged energy $\Omega_{state\text{-}ave}$ given below is taken with respect to the matrix elements of the spinor unitary rotation matrix and configuration mixing coefficients $\{C_{IK}\}$, leading to the Newton-Raphson equations for second-order MCDFB SCF [21]. This state-averaged second-order MCDFB equation yields a single set of spinors for the ground and low-lying even- and odd-parity excited $(\gamma,\mathcal{J},\pi)$ levels, including $^{2S+1}L_{\mathcal{J}}$ fine-structure states:

$$\Omega_{state\text{-}ave} = \sum_{\gamma_K \mathcal{J}\pi} E^{MC}(\gamma_K \mathcal{J}\pi) = \sum_{\gamma_K \mathcal{J}\pi} \sum_{IJ}^{\mathfrak{P}(+)} C_{IK} C_{JK} \langle \Phi_I^{(+)}(\gamma_I \mathcal{J}\pi) | H_{DCB}^{+} | \Phi_J^{(+)}(\gamma_J \mathcal{J}\pi) \rangle, \tag{5}$$

where the summation indices γ, $\mathcal{J}$, and π run over the ground and excited states including a set of $^{2S+1}L_{\mathcal{J}}(\mathcal{J}=|L-S|,\ldots,|L+S|)$ fine-structure states. S and L are the spin and orbital angular momentum quantum numbers.

Conventional state-specific MCDFB SCF has the disadvantage that each state optimized by the MCDFB SCF has its own set of core and valence spinors, which tends to provide the subsequent state-specific second-order perturbation calculations a slightly unbalanced representation of the dynamic correlation corrections to term energy separations. This small imbalance in representing dynamic correlation among states in finite-order perturbation theory prevents an accurate prediction of term energy separations. Note that in all-order perturbation theory, this imbalance would vanish. In contrast, the state-averaged MCDFB SCF has the advantage of defining a single set of spinors for all states included in the state-averaged MCDFB SCF. The single set of spinors provides, in finite-order perturbation theory, a well-balanced representation of dynamic correlation energy corrections on term energy separations. In recent CI+second-order MBPT calculations on two-valence-electron systems [19], a single set of spinors generated by the V^{N-2} potential is employed to accurately account for nondynamic correlation by valence-shell CI and the remaining dynamic correlation by second-order MBPT. Fock-space relativistic coupled cluster theory [24] also employs a single set of spinors generated by the V^{N-2} potential in closed-shell Dirac-Fock calculations. In n (>2) valence-electron systems such as the Fe XI–Fe XIII, however, the closed V^{N-n} core potential yields core spinors that are bound too strongly and thus no longer provides a good lowest-order description. For multivalence-electron systems, a set of core and valence spinors generated in the field of the V^N potential in state-averaged MCDFB SCF provides an excellent lowest-order description [11,25].

B. Multireference CI to account for near degeneracy in highly excited levels

In order to account for strong configuration mixing among the highly excited levels of $n=3$ and 4 manifolds, the configuration interaction method [17–21] is introduced in an extended subspace $\mathfrak{P}_{CI}^{(+)}$ of positive-energy space. N-electron eigenfunctions of the no-pair DCB Hamiltonian are approximated by a linear combination of M_{CI} ($\gg M_{MC}$) configuration-state functions $\{\Phi_I^{(+)}(\gamma_I \mathcal{J}\pi); I=1,2,\ldots,M_{CI}\}$, constructed from the one-particle positive-energy spinors of $n=3$ and 4 manifolds computed in matrix MCDFB SCF. Variation of the configuration-state coefficients $\{C_{IK}\}$ leads to the determinantal CI equation

$$\det[\langle \Phi_I^{(+)}(\gamma_I \mathcal{J}\pi) | H_{DCB}^{+} | \Phi_I^{(+)}(\gamma_I \mathcal{J}\pi) \rangle - E^{CI} \langle \Phi_J^{(+)}(\gamma_J \mathcal{J}\pi) | \Phi_J^{(+)} \times (\gamma_J \mathcal{J}\pi) \rangle] = 0. \tag{6}$$

The eigenfunctions $\{\psi_K^{CI}(\gamma_K \mathcal{J}\pi)\}$ form a subspace $\mathfrak{P}_{CI}^{(+)}$ of the positive-energy space $\mathfrak{D}^{(+)}$:

$$\psi_K^{CI}(\gamma_K \mathcal{J}\pi) = \sum_{I}^{M_{CI}} C_{IK} \Phi_I^{(+)}(\gamma_I \mathcal{J}\pi), \quad K = 1,2,\ldots,M_{CI}. \tag{7}$$

The total DCB energy of the general CI state $|\psi_K^{CI}(\gamma_K \mathcal{J}\pi)\rangle$ can be expressed as

$$E_K^{CI}(\gamma_K \mathcal{J}\pi) = \langle \psi_K^{CI}(\gamma_K \mathcal{J}\pi) | H_{DCB}^{+} | \psi_K^{CI}(\gamma_K \mathcal{J}\pi) \rangle = \sum_{I,J=1}^{\mathfrak{P}_{CI}(+)} C_{IK} C_{JK} \langle \Phi_I^{(+)}(\gamma_I \mathcal{J}\pi) | H_{DCB}^{+} | \Phi_J^{(+)}(\gamma_J \mathcal{J}\pi) \rangle. \tag{8}$$

Here it is assumed that $\psi_K^{CI}(\gamma_K \mathcal{J}\pi)$ and $\Phi_I^{(+)}(\gamma_I \mathcal{J}\pi)$ are normalized.

C. State-specific MR-MP theory for residual correlation corrections

The no-pair DCB Hamiltonian H_{DCB}^{+} is decomposed into two parts, unperturbed Hamiltonian H_0 and perturbation V, following Møller and Plesset [26,27]:

$$H_{DCB}^{+} = H_0 + V. \tag{9}$$

Here the unperturbed model Hamiltonian H_0 is a sum of one-body operators,

$$F_{av} = \sum_{p \in D(+)} |\phi_{n_p \kappa_p}^{(+)}\rangle \langle \phi_{n_p \kappa_p}^{(+)} | f_{av} | \phi_{n_p \kappa_p}^{(+)} \rangle \langle \phi_{n_p \kappa_p}^{(+)}|$$

defined in Refs. [11,16,25].

The N-electron wave functions we seek to refine by MR-MP theory may be expanded in a set of CSF's that spans the entire N-electron positive-energy space $\mathfrak{D}^{(+)}$, $\{\Phi_I^{(+)}(\gamma_I \mathcal{J}\pi)\}$, constructed in terms of Dirac one-electron spinors. Individual CSF's are eigenfunctions of the total angular momentum and parity operators and are linear combinations of antisymmetrized products of positive-energy spinors ($\in D^{(+)}$). The one-electron spinors are mutually orthogonal so the CSF's $\{\Phi_I^{(+)}(\gamma_I \mathcal{J}\pi)\}$ are mutually orthogonal. The unperturbed Hamiltonian is diagonal in this space,

$$H_0 = \sum_{I}^{\mathfrak{D}(+)} |\Phi_I^{(+)}(\gamma_I \mathcal{J}\pi)\rangle E_I^{CSF} \langle \Phi_I^{(+)}(\gamma_I \mathcal{J}\pi)|, \tag{10}$$

so that

$$H_0 |\Phi_I^{(+)}(\gamma_I \mathcal{J}\pi)\rangle = E_I^{CSF} |\Phi_I^{(+)}(\gamma_I \mathcal{J}\pi)\rangle \quad (I = 1,2,\ldots). \tag{11}$$

Since the zero-order Hamiltonian is defined as a sum of one-electron operators F_{av}, E_I^{CSF} is a sum of the products of one-electron energies defined by ε_q^{+} and an occupation number $n_{n_q \kappa_q}[I]$ of the κ_q-symmetry shell in the CSF $\Phi_I^{(+)}(\gamma_I \mathcal{J}\pi)$ [11,16,25]:

$$E_I^{CSF} = \sum_q^{D(+)} \varepsilon_q^+ n_{n_q\kappa_q}[I]. \tag{12}$$

The subset $\{\Phi_I^{(+)}(\gamma_I\mathcal{J}\pi); I=1,2,\ldots,M_{CI}\}$ with which we expand the CI wave function $\psi_K^{CI}(\gamma_K\mathcal{J}\pi)$ [Eq. (7)] also defines an active subspace $\mathfrak{P}_{CI}^{(+)}$ spanned by $\psi_K^{CI}(\gamma_K\mathcal{J}\pi)$ and its $M_{CI}-1$ orthogonal complements $\{\psi_K(\gamma_K\mathcal{J}\pi); K=1,2,\ldots,M_{CI}\}$. The matrix of H_{DCB}^+ in this subspace is diagonal:

$$\langle\psi_K^{CI}(\gamma_K\mathcal{J}\pi)|H_{DCB}^+|\psi_L^{CI}(\gamma_L\mathcal{J}\pi)\rangle = \delta_{KL}(E_K^{(0)}+E_K^{(1)}) = \delta_{KL}E_K^{CI}(\gamma_K\mathcal{J}\pi), \tag{13}$$

where

$$E_K^{(0)} = \langle\psi_K^{CI}(\gamma_K\mathcal{J}\pi)|H_0|\psi_K^{CI}(\gamma_K\mathcal{J}\pi)\rangle = \sum_I^M C_{IK}C_{IK}E_I^{CSF} \tag{14}$$

and

$$E_K^{(1)} = \langle\psi_K^{CI}(\gamma_K\mathcal{J}\pi)|V|\psi_K^{CI}(\gamma_K\mathcal{J}\pi)\rangle. \tag{15}$$

The residual space in the positive-energy subspace is $\mathfrak{Q}^{(+)} = \mathfrak{D}^{(+)} - \mathfrak{P}_{CI}^{(+)}$, which is spanned by CSF's $\{\Phi_I^{(+)}(\gamma_I\mathcal{J}\pi); I=M_{CI}+1, M_{CI}+2,\ldots\}$.

Application of Rayleigh-Schrödinger perturbation theory provides order-by-order expressions of the perturbation series for the state approximated by $|\psi_K^{CI}(\gamma_K\mathcal{J}\pi)\rangle$:

$$E_K(\gamma_K\mathcal{J}\pi) = E_K^{CI}(\gamma_K\mathcal{J}\pi) + E_K^{(2)} + \cdots, \tag{16}$$

where

$$E_K^{(2)} = \langle\psi_K(\gamma_K\mathcal{J}\pi)|V\mathcal{R}V|\psi_K(\gamma_K\mathcal{J}\pi)\rangle. \tag{17}$$

Here, $\mathcal{R}$ is the resolvent operator:

$$\mathcal{R} = \frac{\mathcal{Q}^{(+)}}{E_K^{CSF} - H_0}, \tag{18}$$

with

$$\mathcal{Q}^{(+)} = \sum_I^{\mathfrak{Q}(+)} |\Phi_I^{(+)}(\gamma_I\mathcal{J}\pi)\rangle\langle\Phi_I^{(+)}(\gamma_I\mathcal{J}\pi)|.$$

The projection operator $\mathcal{Q}^{(+)}$ projects onto the subspace $\mathfrak{Q}^{(+)}$ spanned by CSF's $\{\Phi_I^{(+)}(\gamma_I\mathcal{J}\pi); I=M_{CI}+1, M_{CI}+2,\ldots\}$. Using the spectral resolution of the resolvent operator acting on $V|\Phi_I^{(+)}(\gamma_I\mathcal{J}\pi)\rangle$, the second-order correction may be expressed as

$$E_K^{(2)} = \sum_{IJ} C_{IK}C_{JK}\langle\Phi_I^{(+)}(\gamma_I\mathcal{J}\pi)|V\mathcal{R}V|\Phi_J^{(+)}(\gamma_J\mathcal{J}\pi)\rangle = \sum_{L=M+1}^{\mathfrak{Q}(+)}\sum_{I,J=1}^{\mathfrak{P}_{CI}(+)} C_{IK}C_{JK}\frac{\langle\Phi_I^{(+)}(\gamma_I\mathcal{J}\pi)|V|\Phi_L^{(+)}(\gamma_L\mathcal{J}\pi)\rangle\langle\Phi_L^{(+)}(\gamma_L\mathcal{J}\pi)|V|\Phi_J^{(+)}(\gamma_J\mathcal{J}\pi)\rangle}{E_J^{CSF}-E_L^{CSF}}. \tag{19}$$

In this form, all perturbation corrections beyond first order describe the residual dynamic correlation correction for the state approximated by the CI wave function $|\psi_K^{CI}(\gamma_K\mathcal{J}\pi)\rangle$.

Summations over the CSF's in Eqs. (10)–(19) are restricted to CSF's ($\in\mathfrak{D}^{(+)}$) constructed from the positive-energy branch ($D^{(+)}$) of the spinors, effectively incorporating into the computational scheme the "no-pair" projection operator $\mathcal{L}_+$ contained in the DCB Hamiltonians. Further, the CSF's $\Phi_L^{(+)}(\gamma_L\mathcal{J}\pi)$ ($\in\mathfrak{Q}^{(+)}$) generated by excitations higher than double, relative to the reference CSF's $\Phi_I^{(+)}(\gamma_I\mathcal{J}\pi)$ ($\in\mathfrak{B}^{(+)}$), do not contribute to the second and third orders because for them $\langle\Phi_I^{(+)}(\gamma_I\mathcal{J}\pi)|V|\Phi_L^{(+)}(\gamma_L\mathcal{J}\pi)\rangle = 0$ and $\langle\Phi_I^{(+)}(\gamma_I\mathcal{J}\pi)|H_{DC}^+|\Phi_L^{(+)}(\gamma_L\mathcal{J}\pi)\rangle = 0$. State-specific MR-MP on each of the states obtained in the CI accounts for both dynamic pair and pair-pair correlations. Consequently, energy converges at the second-order level, yielding highly accurate term energies for a wide range of excited levels.

III. COMPUTATION

The large and small radial components of the Dirac spinors of symmetry κ are expanded in sets of even-tempered Gaussian-type functions (GTF's) that satisfy the boundary conditions associated with the finite nucleus [28]. The speed of light is taken to be 137. 035 989 5 a.u. throughout this study. The GTF's that satisfy the boundary conditions associated with the finite nucleus are automatically kinetically balanced [28]. Even-tempered basis sets of $26s24p20d18f15g15h15i15j$ G spinors were employed. The order of the partial-wave expansion ($L_{\max}$), the highest angular momentum of the spinors included in the virtual space, is $L_{\max}=7$ throughout this study. The nuclei were modeled as spheres of uniform proton charge in all calculations. Atomic mass for the Fe^{12+} ion is 55.847.

The state-averaged MCDFB SCF for the ground and low-lying excited $\mathcal{J}=0-4$ states in Fe XIII were carried out including 64 even- and odd-parity CSF's arising from the $3s^23p^2$, $3s3p^3$, $3s^23p3d$, and $3s^23p4l$ ($l=0-3$) configurations. Subsequent CI includes all the CSF's arising from the configurations $3s^m3p^n3d^q$ with $m+n+q=4$ (complete active space of the $n=3$ manifold) and $3s^m3p^n3d^q4l$ ($l=0-3$) with $m+n+q=3$ to ensure that the $n=3$ and 4 eigenstates of the matrix CI equation are upperbounds to the exact DCB ener-

gies. A total of 4049 CSF's of $\mathcal{J}=0-5$ (2029 even-parity and 2020 odd-parity CSF's) thus produced were included in the CI calculations. Subsequently, each of the 4049 eigenstates was subjected to state-specific MR-MP refinement to account for residual dynamic correlation. All electrons have been included in the MR-MP perturbation theory calculations to calculate accurately the effects of relativity on electron correlation. MR-MP correlation energy contributions to transition energies from partial wave $L_{max}=8$ and higher are on the order of 10 cm^{-1}. The residual correlation contributions are negligibly small for large $n=4\rightarrow n=3$ transition energies that range from 1 500 000 to 2 000 000 cm^{-1}. For the low-lying states arising from the $3s^23p^2$ configuration, however, the residual correlation contributions are no longer negligible, accounting for up to 0.03% of term energy separations.

Radiative corrections, Lamb shifts, were estimated for each state by evaluating the electron self-energy and vacuum polarization following an approximation scheme discussed by Indelicato, Gorceix, and Desclaux [29]. The code described in Refs. [29,30] was adapted to our basis set expansion calculations for this purpose: All the necessary radial integrals were evaluated analytically. In this scheme [30], the screening of the self-energy is estimated by integrating the charge density of a spinor to a short distance from the origin, typically 0.3 Compton wavelength. The ratio of the integral computed with an MCDFB SCF spinor and that obtained from the corresponding hydrogenic spinor is used to scale the self-energy correction for a bare nuclear charge that has been computed by Mohr [31].

IV. RESULTS AND DISCUSSIONS

A. Term energies of the excited $3s^23p4l$ ($l=0-3$) and $3s3p^24s$ levels

In Table I, theoretical MR-MP term energies of the 54 excited states arising from the $3s^23p4l$ ($l=0-3$) and $3s3p^24s$ configurations are compared with available experimental data [9,10,32]. Term energies of a total of 156 excited levels arising from the $3s3p^24p$, $3s3p^24d$, and $3s3p^24f$ configurations are too voluminous to include here. They are available as supplementary data [33]. The term energies were computed by subtracting the total energy of the ground $\mathcal{J}=0$ ($3s^23p^2\ ^3P_0$) state from the total energies of the excited levels. Values in parentheses adjacent to the term energies are the percentage deviations between experiment and MR-MP theory. Of the computed 54 excited levels, only 25 are experimentally determined. These experimental term energies, taken from the CHIANTI Atomic Database [32] and from experiments by Fawcett *et al.* [9] and Kastner *et al.* [10], are reproduced in the last three columns for comparison. Level numbers of the 25 states are assigned in the third column of the table. None of the excited levels arising from the $3s3p^24s$ configuration has been experimentally identified.

The MR-MP term energies demonstrate that theory deviates from experiment at the 0.01% level for 14 levels. The other 11 levels display deviations ranging from 0.13% to 2.7%. The theoretical term energies are accurate enough that scrutiny of experimental results is warranted when deviations are 0.1% or larger. Deviations (in cm^{-1}) between theory and experiment for the 25 excited levels are plotted against the level numbers in Fig. 1 to exemplify the accuracy of the MR-MP theory and display notable discrepancies. Among the excited levels that exhibit significant deviations are the $3s^23p4s\ ^3P^o_{0,2}$, $3s^23p4p\ ^3D_{1,2}$, $^1P_1$, $3s^23p4d\ ^3P^o_0$ and $3s^23p4f\ ^3G_3$, $^1F_3$, $^3F_4$,$^1D_2$ states where theory deviates from experiment by as much as 0.21%–2.7%. For all these levels, theory indicates that the experimental line identifications [9,10] based on semiempirical calculations are in error (see Sec. III C). We expect the theoretical prediction of all 54 excited levels to be accurate to the 0.01% level.

B. Term energies of $n=3$ levels

In Table II, a detailed comparison of theoretical and experimental data (taken from the CHIANTI atomic database [32]) is made on the term energies of the ground $3s^23p^2\ ^3P_0$ and lowest 26 excited states of Fe XIII [7]. Theoretical term energies of the 70 even-parity levels arising from the $3s3p^23d$ and $3s^23d^2$ configurations are available as supplementary data [33]. None of these 70 excited levels are experimentally observed. Values in parentheses adjacent to the term energies are again the percentage deviations between experiment and MR-MP theory. Experimental term energies and fine-structure intervals compiled in the CHIANTI atomic database [32] are reproduced in the last two columns for comparison. Among the excited levels that exhibit significant deviations are the $3s^23p3d\ ^3F^o_{2,3,4}$ states where theory deviates from experiment by as much as 0.6%. Here the experimental transition energies [34] adopted in the CHIANTI database are in error. A recent fast-beam spectroscopy experiment by Träbert [6] reported the photon wavelength of a radiative transition from the $^3F^o_3$ level that corroborates our theoretical values. The wavelength of the radiative transition $^3F^o_3-{}^3P^o_2$ computed by our MR-MP is 239.05 Å. While approximate, the photon wavelength of 239.2 Å reported by Träbert [6] is in much better agreement with theory than the wavelength of 237.61 Å adopted in the CHIANTI database. We expect that these term energies are accurate to the 0.01% level. Contributions to the term energy separations from the frequency-dependent Breit interaction and mass polarization unaccounted for in this study are estimated at the 0.01% level. Higher accuracy in term energies could be achieved by including these corrections.

C. Wavelengths of the $n=4\rightarrow n=3$ transitions

In Table III, a detailed comparison of the theoretical and experimental data is made for the photon wavelengths associated with the $E1$ radiative decay of the $3s^23p4l$ ($l=0-2$) excited states to the lower $n=3$ states in Fe XIII. Theoretical wavelengths (λ_{theory}) were evaluated from the term energy separations between the upper and lower levels. $E1$ decay rates associated with the transitions are given in the fourth column. Only the transitions with the $E1$ decay rates greater than 2.0×10^{10} s^{-1} are included in the table. Solar lines that match theoretical wavelengths are displayed in the fifth column. New solar line identifications based on our theoretical wavelengths are marked "new" in parentheses adjacent to the

TABLE I. Comparison with experiment of calculated MR-MP term energies (cm^{-1}) of the levels arising from the $3s^23p4s$, $3s^23p4p$, and $3s^23p4d$ configurations.

State	MR-MP	Level number	CHIANTI	Fawcett	Kastner
Odd-parity	$3s^23p4s$ states				
$^3P_0^o$	1334520 (0.55)	1	1327194		
$^3P_1^o$	1336008 (0.02)	2		1336229	
$^3P_2^o$	1351875 (0.21)	3		1354687	
$^1P_1^o$	1360043 (0.13)	4	1361852	1361835	
Even-parity	$3s^23p4p$ states				
$^3S_1$	1437571				
$^3P_1$	1450253				
$^3P_2$	1451602				
$^3P_0$	1456821				
$^3D_1$	1463759 (1.51)	5		1442008	
$^3D_3$	1465585 (0.03)	6		1466036	
$^3D_2$	1470742 (1.30)	7		1451896	
$^1P_1$	1474237 (2.71)	8		1515264[a]	
$^1D_2$	1487561 (0.04)	9		1488107	
$^1S_0$	1516015				
Even-parity	$3s3p^24s$ states				
$^5P_1$	1558408				
$^5P_2$	1565851				
$^5P_3$	1574571				
$^3P_0$	1587880				
$^3P_1$	1592965				
$^3P_2$	1601917				
$^3D_1$	1635753				
$^3D_2$	1636678				
$^3D_3$	1638446				
$^1D_2$	1649299				
$^3S_1$	1701553				
b^3P_0	1714381				
b^3P_1	1728898				
b^3P_2	1736714				
$^1S_0$	1734773				
$^1P_1$	1741928				
Odd-parity	$3s^23p4d$ states				
$^1D_2^o$	1602320				
$^3D_1^o$	1603224 (0.03)	10			1603772
$^3D_2^o$	1603832 (0.02)	11	1604711	1604355	1604200
$^3D_3^o$	1605972 (0.05)	12	1606373	1606499	1606800
$^3F_2^o$	1618783				
$^3F_3^o$	1620817 (0.08)	13			1619592
$^3F_4^o$	1626568				
$^3P_2^o$	1628591 (0.02)	14			1628899
$^3P_1^o$	1630012				
$^1F_3^o$	1629624 (0.06)	15		1630572	1630650
$^3P_0^o$	1633246 (0.84)	16			1619612[a]
$^1P_1^o$	1650379 (0.03)	17			1650850
Even-parity	$3s^23p4f$ states				
$^3G_3$	1700795 (0.55)	18		1703041[a]	1691500[a]
$^1F_3$	1705387 (0.18)	19			1702300[a]
$^3G_4$	1706892 (0.02)	20		1706424[a]	1706585
$^3F_2$	1708075				

TABLE I. (*Continued.*)

State	MR-MP	Level number	CHIANTI	Fawcett	Kastner
$^3F_3$	1718312				
$^3F_4$	1720501 (0.47)	21		1741295	1728539[a]
$^3G_5$	1721872 (0.01)	22		1721461	1721624
$^3D_3$	1728002				
$^3D_2$	1731061				
$^3D_1$	1734106 (0.02)	23			1733745[a]
$^1G_4$	1743950 (0.02)	24		1743895	1743600
$^1D_2$	1745440 (0.25)	25			1741100

[a]Tentative identification.

wavelengths. Solar lines marked "fe12" are those characterized experimentally as the Fe XIII lines. Observed laboratory lines (in Å) by Fawcett *et al.* [9] and by Kastner *et al.* [10] are given in the last two columns. Spectroscopic assignments are made on the four unclassified laboratory lines by Fawcett *et al.* and another by Kastner *et al.* based on our theoretical wavelengths. Theory-experiment deviations for all these five lines are on the order of 0.01 Å.

Kastner *et al.* [10] identified an observed line at 62.10 Å as the $3s^23p4d\ ^3P_0^o \rightarrow 3s^23p^2\ ^3P_1$ decay line, but the wavelength differs significantly from theory and from another laboratory 61.659-Å line identified by Fawcett *et al.* We argue that the line identification by Kastner *et al.* is in error. In fact, the misidentified 62.10-Å line agrees well with the theoretical 62.111-Å and experimental 62.099-Å lines associated with the $3s^23p4d\ ^3P_2^o \rightarrow 3s^23p^2\ ^3P_2$ decay. The experimental term energy of the $3s^23p3d\ ^3P_0^o$ level adopted in the CHIANTI database is based on the misidentified line, result-

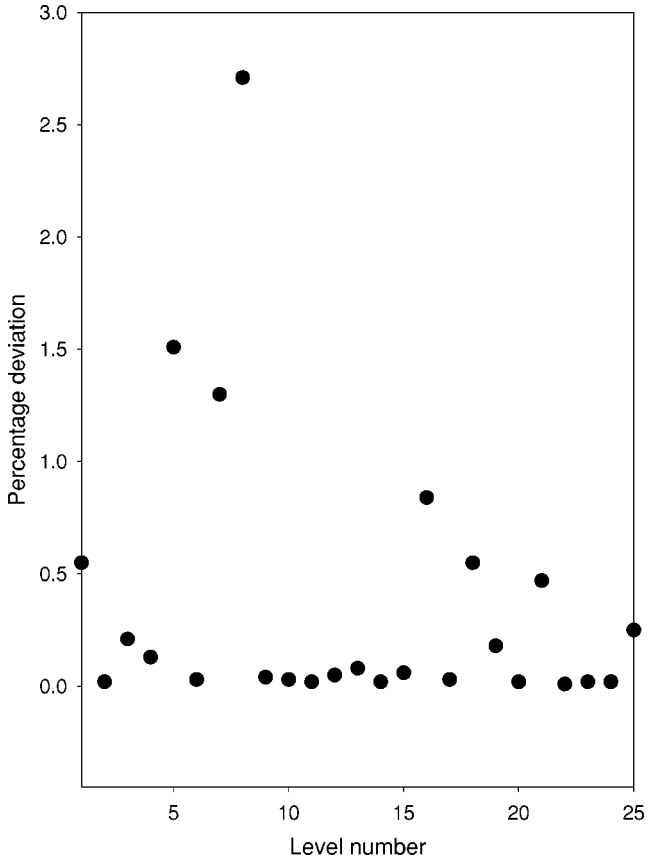

FIG. 1. Percentage deviations between calculated and experimental term energies.

TABLE II. Comparison between calculated and experimental term energies (cm^{-1}) of the levels arising from the $3s^23p^2$, $3s3p^3$, and $3s^23p3d$ configurations.

State	MR-MP		CHIANTI	
	ΔE	FS	ΔE	FS
$3s^23p^2$				
$^3P_0$	0(0.00)	0	0	0
$^3P_1$	9295(0.12)	9295	9306	9306
$^3P_2$	18576(0.05)	18576	18567	18567
$^1D_2$	47985(0.17)		48068	
$^1S_0$	91508(0.00)		91508	
$3s3p^3$				
$^5S_2^o$	214540(0.04)		214624	
$^3D_1^o$	287199(0.00)	0	287205	0
$^3D_2^o$	287348(0.00)	149	287360	155
$^3D_3^o$	290179(0.00)	2980	290180	2975
$^3P_0^o$	328980(0.02)	0	328925	0
$^3P_1^o$	329702(0.00)	722	329706	781
$^3P_2^o$	330334(0.02)	1354	330279	1354
$^1D_2^o$	362416(0.00)		362407	
$^3S_1^o$	415519(0.02)		415462	
$^1P_1^o$	438005(0.01)		438050	
$3s^23p3d$				
$^3F_2^o$	430129(0.60)	0	432741	0
$^3F_3^o$	436905(0.57)	6776	439420	6679
$^3F_4^o$	446959(0.37)	16830	448599	15858
$^3P_2^o$	486403(0.01)	0	486358	0
$^3P_1^o$	495242(0.06)	8839	494942	8584
$^3P_0^o$	501667(0.03)	15264	501520	15162
$^1D_2^o$	498925(0.01)		498870	
$^3D_1^o$	506681(0.04)	0	506502	0
$^3D_2^o$	509479(0.04)	2798	509250	2748
$^3D_3^o$	509441(0.05)	2760	509176	2674
$^1F_3^o$	557303(0.08)		556870	
$^1P_1^o$	571187(0.09)		570690	

TABLE III. Comparison with experiment of theoretical wavelengths of the strongest $E1$ emission lines.

λ_{theory} (Å)	Lower level	Upper level	A (10^{10} s^{-1})	Solar line (Å)	Fawcett	Kastner
	$3s^23p^2$	$3s^23p4d$				
61.578	$^3P_1$	$^3P_0^o$	18.084	61.660 (Si8)	61.659[a]	62.10[b]
61.701	$^3P_1$	$^3P_1^o$	9.420			
62.056	$^3P_2$	$^3P_1^o$	7.035			
62.111	$^3P_2$	$^3P_2^o$	14.697		62.099[a]	
62.132	$^3P_1$	$^3F_2^o$	5.871			
62.374	$^3P_0$	$^3D_1^o$	23.219	62.353 (new)	62.354[a]	62.353
62.413	$^3P_2$	$^3F_3^o$	11.023		62.466[a]	62.46
62.492	$^3P_2$	$^3F_2^o$	3.329			
62.714	$^3P_1$	$^3D_2^o$	21.189	62.680 (fe12)	62.694	62.699
62.738	$^3P_1$	$^3D_1^o$	9.293			62.72[a]
62.996	$^3P_2$	$^3D_3^o$	22.957	62.980 (fe12)	62.975	62.963
63.226	$^1D_2$	$^1F_3^o$	37.435		63.191	63.188
63.267	$^1D_2$	$^3P_2^o$	4.352			
63.580	$^1D_2$	$^3F_3^o$	5.573			
63.662	$^1D_2$	$^3F_2^o$	2.255			
64.149	$^1S_0$	$^1P_1^o$	25.141	64.147 (new)		64.139
64.336	$^1D_2$	$^1D_2^o$	8.098	64.340 (new)		
64.998	$^1S_0$	$^3P_1^o$	3.093			
	$3s^23p^2$	$3s^23p4s$				
74.439	$^3P_1$	$^3P_2^o$	3.865		74.327	
74.850	$^3P_0$	$^3P_1^o$	4.680			
74.957	$^3P_2$	$^3P_2^o$	10.689	74.900 (new)	74.845	
75.374	$^3P_1$	$^3P_1^o$	3.285	75.370 (new)		
75.459	$^3P_1$	$^3P_0^o$	16.050	75.469 (new)		
75.905	$^3P_2$	$^3P_1^o$	7.858	75.879 (fe12,new)	75.892	
76.216	$^1D_2$	$^1P_1^o$	16.348	76.116 (fe12)	76.117	
78.831	$^1S_0$	$^1P_1^o$	2.906			
	(a)$3s3p^3$ (b)$3s^23p3d$	$3s^23p4p$				
85.498	(a) $^3D_1^o$	$^3P_0$	2.944			
96.727	(b) $^3F_3^o$	$^3D_2$	0.231		98.523	
96.746	(b) $^3F_2^o$	$^3D_1$	0.319		98.826	
98.027	(b) $^3F_2^o$	$^3P_1$	2.311			
98.171	(b) $^3F_4^o$	$^3D_3$	4.329		98.128	
98.552	(b) $^3F_3^o$	$^3P_2$	4.082	98.517 (new)		
99.261	(b) $^3F_2^o$	$^3S_1$	2.267			
102.531	(b) $^1D_2^o$	$^1P_1$	0.384		98.387[b]	
103.996	(b) $^3P_1^o$	$^3P_0$	2.228			
105.839	(b) $^1P_1^o$	$^1S_0$	3.252	105.820 (new)		
107.497	(b) $^1F_3^o$	$^1D_2$	2.399		107.384	

[a]Unclassified observed line.
[b]Tentative identification.

ing in large theory-CHIANTI percentage deviation of 0.84%. A solar line at 61.660 Å is in excellent agreement with the laboratory 61.659-Å line associated with the $3s^23p4d\ ^3P_0^o \rightarrow 3s^23p^2\ ^3P_1$ decay, although it is attributed to a Si IX decay line (thus marked "Si8" in parentheses). We argue that the Fe XIII line is blended with the intense Si IX line observed in solar flares.

Theoretical photon wavelength of 74.439 Å associated with the $3s^23p4s\ ^3P_2^o \rightarrow 3s^23p^2\ ^3P_1$ decay deviates noticeably from the experimental wavelength of 74.327 Å classified by Fawcett *et al.* This difference entails the theory-experiment percentage deviations of 0.21% in the $3s^23p4s\ ^3P_2^o$ term energy (Table I). The source of the discrepancy is not immediately apparent.

TABLE IV. Wavelengths of the strongest $E1$ emission lines originating from the even-parity $3s^2 2p4f$ states to the odd-parity $3s3p^3$ and $3s^2 3p3d$ states.

λ_{theory} (Å)	Lower level	Upper level	A (10^{10} s^{-1})	Solar line (Å)	Fawcett	Kastner
	(a) $3s3p^3$	$3s^2 3p4f$				
	(b) $3s^2 3p3d$					
69.883	(a) $^3D^o_2$	$^3F_3$	2.716			
69.914	(a) $^3D^o_3$	$^3F_4$	4.517			
70.370	(a) $^3D^o_1$	$^3F_2$	7.048	70.340 (new)		
70.520	(a) $^3D^o_2$	$^1F_3$	4.862	70.545 (new)		
70.586	(a) $^3D^o_3$	$^3G_4$	3.249			
71.168	(a) $^3P^o_0$	$^3D_1$	3.487			
71.205	(a) $^3P^o_1$	$^3D_1$	3.520			
71.359	(a) $^3P^o_1$	$^3D_2$	4.527	71.374 (new)		
71.392	(a) $^3P^o_2$	$^3D_2$	2.360			
71.548	(a) $^3P^o_2$	$^3D_3$	4.761			
72.305	(a) $^1D^o_2$	$^1D_2$	4.524			
73.229	(a) $^1D^o_2$	$^3D_3$	2.349			
73.752	(a) $^1D^o_2$	$^3F_3$	5.874			
74.462	(a) $^1D^o_2$	$^1F_3$	3.720			74.629
74.717	(a) $^1D^o_2$	$^3G_3$	14.243	74.630 (ne7)[a]		75.241
76.486	(a) $^1P^o_1$	$^1D_2$	4.949			
77.629	(b) $^3F^o_2$	$^3F_3$	14.102			
77.906	(b) $^3F^o_3$	$^3F_4$	16.165	77.920 (new)		
78.039	(b) $^3F^o_3$	$^3F_3$	7.364			
78.240	(b) $^3F^o_2$	$^3F_2$	5.347			
78.416	(b) $^3F^o_2$	$^1F_3$	16.309			
78.437	(b) $^3F^o_4$	$^3G_5$	65.464	78.470 (mg7)	78.462	78.452
78.521	(b) $^3F^o_4$	$^3F_4$	10.617			
78.699	(b) $^3F^o_2$	$^3G_3$	30.503	78.714 (new)	78.56[b]	
78.741	(b) $^3F^o_3$	$^3G_4$	44.741	78.729 (new)	78.77[c]	78.760
79.121	(b) $^3F^o_3$	$^3G_3$	2.208			
80.224	(b) $^1D^o_2$	$^1D_2$	4.279			
80.343	(b) $^3P^o_2$	$^3D_2$	2.804			
80.541	(b) $^3P^o_2$	$^3D_3$	11.357	80.503 (fe11)	80.5(fe11)[d]	
80.719	(b) $^3P^o_1$	$^3D_1$	5.624			
80.918	(b) $^3P^o_1$	$^3D_2$	17.064			
81.140	(b) $^3P^o_0$	$^3D_1$	26.849	81.140 (new)		81.154
81.362	(b) $^1D^o_2$	$^3D_2$	10.993			
81.471	(b) $^3D^o_1$	$^3D_1$	20.339	81.540 (fe19)		
81.658	(b) $^3D^o_2$	$^3D_1$	3.471			
81.674	(b) $^3D^o_1$	$^3D_2$	14.867		81.651(fe11)[d]	
81.843	(b) $^3P^o_2$	$^3D_2$	2.369			
81.861	(b) $^3D^o_2$	$^3D_2$	17.712	81.860 (new)		
82.008	(b) $^1D^o_2$	$^3F_3$	20.524	81.940 (new)		
82.036	(b) $^3P^o_2$	$^1F_3$	25.256			
82.064	(b) $^3D^o_3$	$^3D_3$	11.362			
82.067	(b) $^3D^o_2$	$^3D_3$	18.444			
82.346	(b) $^3D^o_2$	$^3G_3$	7.260			
82.440	(b) $^3P^o_1$	$^3F_2$	24.686	82.418 (fe8)		
82.572	(b) $^3D^o_3$	$^3F_4$	31.065		81.161	82.010
82.724	(b) $^3D^o_2$	$^3F_3$	9.430	82.763 (new)		
83.204	(b) $^1D^o_2$	$^3G_3$	5.943			
83.224	(b) $^3D^o_1$	$^3F_2$	18.386	83.230 (new)		
83.511	(b) $^3D^o_3$	$^3G_4$	14.915	83.446 (fe8)		
83.619	(b) $^3D^o_2$	$^1F_3$	10.144	83.620 (new)		
84.271	(b) $^1F^o_3$	$^1G_4$	56.051		84.275	84.270
85.161	(b) $^1P^o_1$	$^1D_2$	41.563		85.14(fe11) [c]	85.461
87.451	(b) $^1F^o_3$	$^3G_3$	2.952			

[a]Unclassified observed line.
[b]Tentative identification.
[c]Blended.
[d]Small transition probability.

TABLE V. Recommended term energies (cm^{-1}) of the levels arising from the $3s^23p4s$, $3s^23p4p$, $3s^23p4d$, and $3s^23p4f$ configurations.

State	Term energy	Source
$3s^23p4s$		
$^3P_0^o$	1334520±400[a]	theory
$^3P_1^o$	1336229±175	75.892-Å line by Fawcett *et al.*
$^3P_2^o$	1351875±405[a]	theory
$^1P_1^o$	1361835±175	76.117-Å line by Fawcett *et al.*
$3s^23p4p$		
$^3P_2$	1451911±150	98.523-Å line by Fawcett *et al.*
$^3D_1$	1463759±439[a]	theory
$^3D_2$	1470742±441[a]	theory
$^3D_3$	1466057±200	98.128-Å line by Fawcett *et al.*
$^1D_2$	1488107±150	107.384-Å line by Fawcett *et al.*
$^1P_1$	1474237±442[a]	theory
$3s^23p4d$		
$^3D_1^o$	1603746±250	62.353-Å line by Kastner *et al.* and 62.354-Å line by Fawcett *et al.*
$^3D_2^o$	1595049±250	62.699-Å line by Kastner *et al.* and 62.694-Å line by Fawcett *et al.*
$^3D_3^o$	1606499±250	62.963-Å line by Kastner *et al.* and 62.975-Å line by Fawcett *et al.*
$^3F_3^o$	1619438±260	62.46-Å line by Kastner *et al.* and 62.466-Å line by Fawcett *et al.*
$^1F_3^o$	1582504±240	63.188-Å line by Kastner *et al.* and 63.191-Å line by Fawcett *et al.*
$^3P_0^o$	1631129±270	61.659-Å line by Fawcett *et al.*
$^3P_2^o$	1628899±260	62.10-Å line by Kastner *et al.* and 62.099-Å line by Fawcett *et al.*
$^1P_1^o$	1650622	64.139-Å line by Kastner *et al.*
$3s^23p4f$		
$^3G_3$	1702369	74.629-Å line by Kastner *et al.*
$^1F_3$	1705387±512[a]	theory
$^3G_4$	1706600	78.760-Å line by Kastner *et al.* and 78.77-Å line by Fawcett *et al.*
$^3F_4$	1720501±516[a]	theory
$^3G_5$	1721482±300	78.452-Å line by Kastner *et al.* and 78.462-Å line by Fawcett *et al.*
$^3D_1$	1733639±150	81.154-Å line by Kastner *et al.* and 81.161-Å line by Fawcett *et al.*
$^1G_4$	1743462±150	84.270-Å line by Kastner *et al.* and 84.275-Å line by Fawcett *et al.*
$^1D_2$	1745226	85.14-Å line by Fawcett *et al.* blended with Fe XII line

[a]0.03% uncertainty in theoretical term energies is assumed.

Theoretical photon wavelength of 75.459 Å deviates significantly from a solar line at 75.879 Å classified by Dere [5] as the $3s^23p4s\ ^3P_0^o \rightarrow 3s^23p^2\ ^3P_1$ transition. This deviation entails the large theory-experiment percentage deviations of 0.55% in the $3s^23p4s\ ^3P_0^o$ term energy. The solar line identification by Dere is clearly in error. In fact, the wavelength of the solar line agrees to the 0.01-Å level with the theoretical wavelength of 75.905 Å as well as with the laboratory 75.892-Å line for the $3s^23p4s\ ^3P_1^o$-$3s^23p^2\ ^3P_2$ transition. Thus, we identify this misidentified solar line at 75.879 Å as the $3s^23p4s\ ^3P_1^o$-$3s^23p^2\ ^3P_2$ transition.

A laboratory line at 98.523 Å was classified by Fawcett *et al.* as the $3s^23p4p\ ^3D_2 \rightarrow 3s^23p3d\ ^3F_3^o$ transition. However, theory places this transition at 96.727 Å, in serious disagreement with the laboratory assignment. Because of this disagreement, the theory-experiment percentage deviation of

TABLE VI. Wavelengths of the strongest $E1$ emission lines originating from the even-parity $3s3p^24s$ to the odd-parity excited $3s3p^3$ and $3s^3p3d$ states.

λ_{theory} (Å)	Lower level	Upper level	A (10^{+10} s^{-1})	Solar line (Å)
	(a) $3s3p^3$	$3s3p^24s$		
	(b) $3s^23p3d$			
72.489	(a) $^1D_2^o$	$^1P_1$	9.079	72.410 (si7)
72.894	(a) $^3P_1^o$	$^3S_1$	3.833	
72.928	(a) $^3P_2^o$	$^3S_1$	7.400	72.899 (new)
73.528	(a) $^5S_2^o$	$^5P_3$	9.474	73.560 (ne7)
74.002	(a) $^5S_2^o$	$^5P_2$	4.661	
74.103	(a) $^3D_1^o$	$^3D_2$	2.565	
74.111	(a) $^3D_2^o$	$^3D_2$	7.181	
74.154	(a) $^3D_1^o$	$^3D_1$	8.029	74.120 (new)
74.162	(a) $^3D_2^o$	$^3D_1$	2.312	
74.169	(a) $^3D_3^o$	$^3D_3$	7.518	
74.412	(a) $^5S_2^o$	$^5P_1$	9.595	74.400 (new)
75.689	(a) $^3S_1^o$	b$^3P_2$	5.337	
76.140	(a) $^3S_1^o$	b$^3P_1$	6.233	76.150 (fe13)
76.235	(a) $^3D_3^o$	$^3P_2$	10.639	
76.567	(a) $^3P_1^o$	$^3D_1$	3.137	
76.592	(a) $^3D_2^o$	$^3P_1$	11.410	
76.692	(a) $^1P_1^o$	$^1P_1$	7.771	
76.883	(a) $^3D_1^o$	$^3P_0$	14.624	76.866 (new)
76.991	(a) $^3S_1^o$	b$^3P_0$	8.453	
77.115	(a) $^1P_1^o$	$^1S_0$	10.473	77.200 (new)
77.707	(a) $^1D_2^o$	$^1D_2$	3.173	
78.642	(a) $^3P_2^o$	$^3P_2$	4.507	
79.480	(a) $^3P_1^o$	$^3P_0$	3.225	
79.648	(b) $^3P_2^o$	$^1P_1$	2.101	
80.450	(b) $^1D_2^o$	$^1P_1$	5.849	80.503 (fe11)

the $3s^23p4p\ ^3D_2$ term energy in Table I is very large, 1.3%. The laboratory line has been clearly misidentified. This 98.523-Å line, which closely matches the theoretical line at 98.552-Å and the newly identified solar line at 98.517 Å, should be attributed to the $3s^23p4p\ ^3P_2 \rightarrow 3s^23p3d\ ^3F_3^o$ transition. Theoretical photon wavelengths 102.531 Å and 96.746 Å associated, respectively, with the $3s^23p4p\ ^1P_1 \rightarrow 3s^23p3d\ ^1D_2^o$ and $3s^23p4p\ ^3D_1 \rightarrow 3s^23p3d\ ^3F_2^o$ transitions differ considerably from the observed wavelengths by Fawcett *et al.*, resulting in large theory-experiment percentage deviations in the $3s^23p4p\ ^1P_1$ and $3s^23p4p\ ^3D_1$ term energies. We argue that these laboratory lines have been misidentified.

Table IV displays theoretical photon wavelengths associated with the 53 strongest $E1$ emissions from the even-parity $3s^23p4f$ levels. Only the transitions with the $E1$ decay rates greater than 2.0×10^{10} s^{-1} are included in the table. Observed laboratory lines by Fawcett *et al.* and Kastner *et al.* are displayed in the last two columns. New solar line identifications are made based on theoretical wavelengths: Hitherto unclassified solar lines that closely match theoretical wavelengths with high $E1$ transition rates are classified and displayed in the fifth column.

TABLE VII. $M1/E2$ transition probabilities (s^{-1}) and lifetimes (ms) of the $3s^23p^2$ states.

Upper state	Type	Lower state $^3P_0$	$^3P_1$	$^3P_2$	$^1D_2$	τ_{theory}	τ_{expt}
$3s^23p^2$							
$^3P_1$	$M1$	13.953				71.67	
$^3P_2$	$M1$		9.964			100.33	
	$E2$	0.003	0.0004				
$^1D_2$	$M1$		58.822	71.998		7.63	8.0 ± 0.1[a]
	$E2$	0.199	0.0373	0.0624			
$^1S_0$	$M1$		974.08			1.021	
	$E2$			3.851	1.642		

[a]Reference [37].

The theoretical wavelength of 74.462 Å, associated with the $3s^23p4f\ ^1F_3 \rightarrow 3s^23p3d\ ^1D_2^o$ transition, deviates noticeably from the observed wavelength of 74.629 Å [10], entailing a theory-experiment percentage deviation of 0.18% in the $3s^23p4f\ ^1F_3$ term energy. The line identification by Kastner *et al.* is suspect. In fact, the observed line agrees better with the theoretical $3s^23p4f\ ^3G_3 \rightarrow 3s^23p3d\ ^1D_2^o$ decay line at 74.717 Å. A solar line at 74.630 Å, identified as the intense Ne^{7+} line, closely matches the laboratory 74.629-Å line. It is likely that the Fe XIII line is blended with the Ne^{7+} line in solar flares. The classification of a laboratory line at 75.241 Å [10] as the $3s^23p4f\ ^3G_3 \rightarrow 3s^23p3d\ ^1D_2^o$ decay line is clearly in error.

A laboratory line at 78.56 Å has been tentatively identified by Fawcett *et al.* as the $3s^23p4f\ ^3G_3 \rightarrow 3s^23p3d\ ^3F_2^o$ decay line. The observed wavelength, however, deviates by more than 0.1 Å from theory. We argue that the line has been erroneously identified. The theoretical $3s^23p4f\ ^3F_4 \rightarrow 3s^23p3d\ ^3F_4^o$ decay line at 78.521 Å agrees within hundredths of an angstrom with the misidentified line. The observed 78.56-Å line is thereby classified as the $3s^23p4f\ ^3F_4 \rightarrow 3s^23p3d\ ^3F_4^o$ decay.

Two laboratory lines, at 80.5 Å and at 81.651 Å, were identified by Fawcett *et al.* as the Fe^{11+} lines. However, theoretical transition rates of both these Fe XII decay lines are, in fact, very small, implying that they are not readily detectable. We argue that the lines are misidentified. We identify the observed 80.5-Å and 81.651-Å lines, respectively, as the Fe XIII $3s^23p4f\ ^3D_3 \rightarrow 3s^23p3d\ ^3P_2^o$ and $3s^23p4f\ ^3D_2 \rightarrow 3s^23p3d\ ^3D_1^o$ transitions. Wavelengths of these observed lines agree within hundredths of an angstrom with theoretical wavelengths of the transitions with large decay rates, 11.4×10^{10}–14.9×10^{10} s^{-1}.

The theoretical wavelength of 82.572 Å deviates significantly from the observed wavelength of 81.161 Å identified as the $3s^23p4f\ ^3F_4 \rightarrow 3s^23p3d\ ^3D_3^o$ transition [9], entailing a theory-experiment percentage deviation of 0.47% in the $3s^23p4f\ ^3F_4$ term energy. The line identification by Fawcett *et al.* is clearly in error. In fact, the observed laboratory line closely matches the theoretical and another experimental

TABLE VIII. Theoretical $E1$ transition probabilities (s^{-1}) and lifetimes (s) of the states in the $3s3p^3$-$3s^23p^2$ and $3s^23p3d$-$3s^23p^2$ transition arrays.

	Lower state $3s^23p^2$					
Upper state	$^3P_0$	$^3P_1$	$^3P_2$	$^1D_2$	$^1S_0$	τ
$3s3p^3$						
$^5S_2^o$		4.381(+6)	7.371(+6)	1.610(+5)		8.395(−8)
$^3D_1^o$	1.199(+9)	3.215(+8)	1.068(+7)	2.478(+7)	2.031(+6)	6.426(−10)
$^3D_2^o$		1.374(+9)	5.027(+7)	8.352(+6)		7.017(−10)
$^3D_3^o$			1.191(+9)	7.445(+7)		7.902(−10)
$^3P_0^o$		3.910(+9)				2.558(−10)
$^3P_1^o$	1.191(+9)	1.757(+9)	8.903(+8)	4.368(+7)	1.912(+7)	2.563(−10)
$^3P_2^o$		4.159(+8)	3.085(+9)	1.005(+7)		2.848(−10)
$^1D_2^o$		6.940(+7)	6.302(+7)	4.914(+9)		1.982(−10)
$^3S_1^o$	6.791(+9)	1.681(+10)	3.209(+10)	6.596(+8)	3.645(+8)	1.763(−11)
$^1P_1^o$	8.015(+8)	4.769(+9)	1.054(+9)	2.855(+10)	4.171(+9)	2.542(−11)
$3s^23p3d$						
$^3F_2^o$		9.865(+7)	1.125(+8)	2.867(+8)		2.009(−9)
$^3F_3^o$			2.741(+8)	2.210(+7)		3.376(−9)
$^3P_2^o$		1.952(+10)	1.777(+10)	1.238(+10)		2.013(−11)
$^3P_1^o$	4.233(+10)	1.041(+6)	8.539(+9)	7.756(+8)	6.127(+7)	1.934(−11)
$^1D_2^o$		1.485(+10)	3.721(+7)	4.154(+10)		1.772(−11)
$^3P_0^o$		4.592(+10)				2.178(−11)
$^3D_1^o$	1.123(+10)	3.998(+10)	1.114(+10)	1.095(+9)	1.723(+7)	1.576(−11)
$^3D_2^o$		2.660(+10)	3.282(+10)	4.681(+9)		1.560(−11)
$^3D_3^o$			6.377(+10)	2.057(+9)		1.519(−11)
$^1F_3^o$			2.928(+9)	6.741(+10)		1.422(−11)
$^1P_1^o$	3.794(+8)	1.326(+8)	1.103(+6)	7.188(+7)	5.506(+10)	1.797(−11)

$3s^23p4f\ ^3D_1 \rightarrow 3s^23p3d\ ^3P_0^o$ decay line at 81.140 Å and at 81.154 Å [10], respectively. An unclassified solar line at 81.140 Å is newly identified as the $3s^23p4f\ ^3D_1 \rightarrow 3s^23p3d\ ^3P_0^o$ decay line. We argue that a laboratory line at 82.010 Å was erroneously identified by Kastner *et al.* as the $3s^23p4f\ ^3F_4 \rightarrow 3s^23p3d\ ^3D_3^o$ transition. Here, the theory-experiment deviation is too large, over 0.5 Å. The observed line, however, agrees well with the theoretical 82.036-Å line, strongly suggesting that it should be attributed to the $3s^23p4f\ ^1F_3 \rightarrow 3s^23p3d\ ^3P_2^o$ transition.

A laboratory line at 85.461 Å was classified [10] as the $3s^23p4f\ ^1D_2 \rightarrow 3s^23p3d\ ^1P_1^o$ transition. However, theoretical wavelength 85.161 Å of this transition deviates by as much as 0.3 Å from the observed line. We argue that the observed laboratory line has been misidentified. The intense $3s^23p4f\ ^1G_4 \rightarrow 3s^23p3d\ ^1F_3^o$ and $3s^23p4f\ ^1D_2 \rightarrow 3s^23p3d\ ^1P_1^o$ transitions have not been observed in the solar spectrum for yet unknown reasons although they have been observed experimentally [9]. The theoretical 85.161-Å line matches an intense laboratory line at 85.14 Å that Fawcett *et al.* identified earlier as a Fe XII line. We argue that the Fe XII line is blended with the Fe XIII line.

Collected in Table V are the recommended term energies of the 26 levels arising from the $3s^23p4l$ ($l=0-3$) configurations based on our theoretical line identifications and critical evaluation of the observed laboratory lines. The estimated uncertainties in theoretical term energies are based on the average theory-experiment percentage deviation of 0.03% over the 14 levels with less than 0.1% theory-experiment deviations (see Sec. IV A). The uncertainties in experimental term energies are based on the error estimate of 0.01 Å in the observed wavelengths [9].

In Table VI, theoretical photon wavelengths assocated with the $E1$ emissions from the even-parity $3s3p^24s$ levels are displayed. Only the transitions with $E1$ decay rates greater than 2.0×10^{10} s^{-1} are included in the table. The $E1$ transitions from a total of 156 excited levels arising from the $3s3p^24p$, $3s3p^24d$, and $3s3p^24f$ configurations are too voluminous to be included here but they are available as supplementary data [33]. There are no laboratory lines to compare with theory. New solar line identifications are made based on our theoretical wavelengths: Hitherto unclassified solar lines that closely match theoretical wavelengths with high $E1$ transition rates are classified and displayed in the fifth column.

Table VII displays theoretical $M1$ and $E2$ decay rates for the transitions from four $3s^23p^2$ upper levels (first column) to lower levels (first row). Theoretical lifetimes are given in the last column of the table. The $M1$ transition probabilities are several orders of magnitude larger than the $E2$ for all four levels, indicating that radiative decays occur predominantly via the $M1$ transition. The theoretical lifetime of the $3s^23p^2\ ^1D_2$ state deviates from experiment by as much as 4 times the experimental uncertainty [9]. Table VIII displays

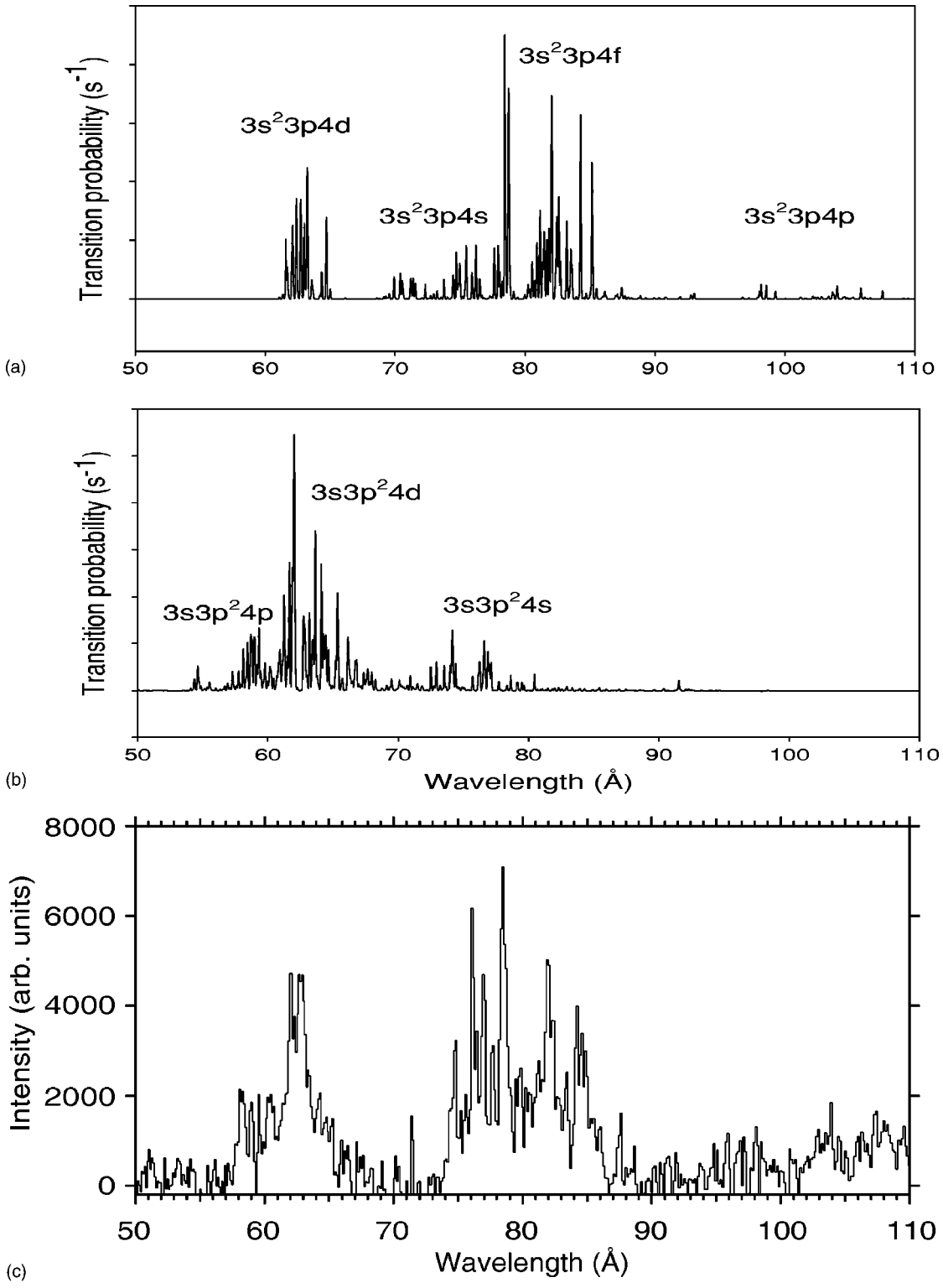

FIG. 2. Observed and synthetic soft-x-ray spectra of the Fe XIII radiative emissions.

theoretical $E1$ transition probabilities and lifetimes of the excited levels arising from the $3s3p^3$ and $3s^23p3d$ configurations. There are no experimental lifetimes available for these levels for comparison. The theoretical lifetimes are a benchmark for future experiments.

D. Synthetic spectrum

Recent experiments [12,35] have provided increasing evidence that the published atomic data used by astronomers are incomplete [12]. The spectral flux for Fe VII–Fe XIII observed with Livermore electron beam ion trap (EBIT) in the EUV

and soft-x-ray wavelength regions indicates serious deficiencies in extant spectral models. The spectral model by Kaastra and Mewe [36] predicts only eight lines in the spectral range of 50–110 Å in Fe XIII, omitting most of the lines Beiersdorfer *et al.* observed [35]. The CHIANTI code performance is even worse, with only four lines in this range.

Our MR-MP theory places well over 1500 $E1$ transitions in this spectral range, a high density of lines that Lepson *et al.* have observed [12]. Figures 2(a) and 2(b) display synthetic soft-x-ray spectra of Fe XIII in the 50–115-Å range based on our theoretical data. The spectra are produced by assuming that the spectral line intensities are proportional to weighted $E1$ transition probabilities and Gaussian line shapes of the form $F(\omega)=A\exp[-(\omega-\lambda_{theory})^2/\Gamma^2]$, where A is the transition probability and $\Gamma=0.05$.

Figure 2(a) displays the emission lines arising from the $3s^23p4l$ ($l=0-3$) levels, Fig. 2(b) from the $3s3p^24l$ ($l=0-2$) levels. Transitions from the $3s3p^24f$ levels do not fall into this spectral range. Theory attributes a high density of lines in the 55–67-Å range in the observed spectrum to the emission lines from the $3s^23p4d$, $3s3p^24p$, and $3s3p^24d$ levels and another set of high density lines appearing between 70 Å and 90 Å to the emission lines from the $3s^23p4s$, $3s3p^24f$, and $3s3p^24s$ levels. Together, the synthetic spectra reproduce the overall feature of the laboratory spectrum [Fig. 2(c)] produced on EBIT [12], although the relative intensity of the two sets of lines are not well reproduced because of lack of information on the population distribution and temperature.

V. CONCLUSION

Multiple openshell systems with more than two valence electrons give complex spectra because of a large number of nearly degenerate multiplet states that arise from multiple open shells. In an earlier study, a relativistic multireference Møller-Plesset (MR-MP) perturbation theory based on the state-averaged MCDFB SCF was implemented and successfully applied to siliconlike argon, aluminumlike iron, and ions of silicon isoelectronic sequence [7,11]. In that study, the state-averaged energy over a number of $n=3$ states was optimized by the MCDFB SCF procedure followed by state-specific second-order MR-MP to obtain highly accurate term energy separations and lifetimes. In the present study, we have successfully generalized the previous study and developed a combined state-averaged MCDFB SCF/CI +state-specific MR-MP procedure to obtain accurate term energies, soft-x-ray transition energies and decay rates of highly excited levels of $n=4$ manifold in multiple-valence-electron systems. Relativistic multireference perturbation calculations have been carried out for a large number of odd- and even-parity $n=4$ excited levels of siliconlike iron to demonstrate the unprecedented accuracy. It can provide accurate UV, EUV, and soft-x-ray transition energies and transition rates for numerous highly excited levels of multivalence-electron atoms for a broad range of ionizations. Our relativistic MR-MP perturbation theory is a theoretical tool for EUV and x-ray spectroscopy that quantitatively demonstrates its accuracy.

ACKNOWLEDGMENTS

We owe special thanks to Dr. P. Beiersdorfer and Dr. J. K. Lepson for providing us with their soft-x-ray spectrum of Fe XIII. This research is supported in part by the U.S.-Israel Binational Science Foundation.

[1] Chandra X-ray observatory. Available at http://chandra.harvard.edu/
[2] The Solar and Heliospheric Observatory. Available at http://sohowww.nascom.nasa.gov/
[3] E. Träbert, A. G. Calamai, G. Gwinner, E. J. Knystautas, E. H. Pinnington, and A. Wolf, J. Phys. B **36**, 1129 (2003).
[4] G. D. Sandlin, J.-D. F. Bartoe, G. E. Brueckner, R. Tousey, and M. E. VanHoosier, Astrophys. J., Suppl. Ser. **61**, 801 (1986).
[5] K. P. Dere, Astrophys. J. **221**, 1062 (1978).
[6] E. Träbert, Mon. Not. R. Astron. Soc. **297**, 399 (1998).
[7] M. J. Vilkas and Y. Ishikawa, J. Phys. B **36**, 4641 (2003).
[8] M. J. Vilkas and Y. Ishikawa, J. Phys. B **37**, 1803 (2004).
[9] B. C. Fawcett, R. D. Cowan, E. Y. Kononov, and R. W. Hayes, J. Phys. B **5**, 1255 (1972).
[10] S. O. Kastner, M. Swartz, A. K. Bhatia, and J. Lapides, J. Opt. Soc. Am. **68**, 1558 (1979).
[11] M. J. Vilkas and Y. Ishikawa, Phys. Rev. A **68**, 012503 (2003).
[12] J. K. Lepson, P. Beiersdorfer, G. V. Brown, S. M. Kahn, D. A. Liedahl, C. W. Mauche, and S. B. Utter, Rev. Mex. Astron. Astrofis. **9**, 137 (2000).
[13] A. W. Weiss and Y.-K. Kim, Phys. Rev. A **51**, 4487 (1995).
[14] E. Avgoustoglou, W. R. Johnson, Z. W. Liu, and J. Sapirstein, Phys. Rev. A **51**, 1196 (1995).
[15] E. Avgoustoglou and D. R. Beck, Phys. Rev. A **57**, 4286 (1998).
[16] M. J. Vilkas, Y. Ishikawa, and K. Koc, Phys. Rev. A **60**, 2808 (1999).
[17] M. H. Chen, K. T. Cheng, and W. R. Johnson, Phys. Rev. A **47**, 3692 (1993).
[18] V. A. Dzuba, V. V. Flambaum, and M. G. Kozlov, Phys. Rev. A **54**, 3948 (1996).
[19] I. M. Savukov and W. R. Johnson, Phys. Rev. A **65**, 042053 (2002).
[20] D. R. Beck, Phys. Rev. A **56**, 2428 (1997).
[21] M. J. Vilkas, Y. Ishikawa, and K. Koc, Phys. Rev. E **58**, 5096 (1998).
[22] J. Sucher, Phys. Rev. A **22**, 348 (1980).
[23] M. H. Mittleman, Phys. Rev. A **24**, 1167 (1981).
[24] E. Eliav, U. Kaldor, and Y. Ishikawa, Phys. Rev. A **49**, 1724 (1994).
[25] Y. Ishikawa and M. J. Vilkas, Phys. Rev. A **63**, 042506 (2001).
[26] C. Møller and M. S. Plesset, Phys. Rev. **46**, 618 (1934).
[27] K. Hirao, Chem. Phys. Lett. **190**, 374 (1992).
[28] Y. Ishikawa, H. M. Quiney, and G. L. Malli, Phys. Rev. A **43**, 3270 (1991).
[29] P. Indelicato, O. Gorceix, and J. P. Desclaux, J. Phys. B **20**,

651 (1987).
[30] Y.-K. Kim, in *Atomic Processes in Plasmas*, edited by Yong Ki-Kim and Raymond C. Elton, AIP Conf. Proc. No. 206 (AIP, New York, 1990), p. 19.
[31] P. J. Mohr, Phys. Rev. A **46**, 4421 (1992).
[32] K. P. Dere, E. Landi, H. E. Mason, B. C. Monsignori Fossi, and P. R. Young, Astron. Astrophys., Suppl. Ser. **125**, 149 (1997). Available online at http://wwwsolar.nrl.navy.mil/chianti.html
[33] Available upon request.
[34] C. Jupén, R. Isler, and E. Träbert, Mon. Not. R. Astron. Soc. **264**, 627 (1993).
[35] P. Beiersdorfer, J. Lepson, G. Brown, S. Utter, S. Kahn, D. Liedahl, and C. Mauche, Astrophys. J. Lett. **519**, L185 (1999).
[36] J. Kaastra and R. Mewe, Legacy **3**, 6 (1993).
[37] E. Träbert, Can. J. Phys. **80**, 1481 (2002).